Binding-site geometry and flexibility in DC-SIGN demonstrated with surface force measurements

Sindhu Menon[a], Kenneth Rosenberg[b,1], Sarah A. Graham[c], Eliot M. Ward[c], Maureen E. Taylor[c], Kurt Drickamer[c], and Deborah E. Leckband[a,b,2]

Departments of [a]Chemistry and [b]Chemical and Biomolecular Engineering, University of Illinois at Urbana–Champaign, 600 South Mathews Avenue, Urbana, IL 61801; and [c]Division of Molecular Biosciences, Department of Life Sciences, Imperial College, London SW7 2AZ, United Kingdom

Edited by Stephen P. Goff, Columbia University College of Physicians and Surgeons, New York, NY, and approved May 15, 2009 (received for review February 16, 2009)

The dendritic cell receptor DC-SIGN mediates pathogen recognition by binding to glycans characteristic of pathogen surfaces, including those found on HIV. Clustering of carbohydrate-binding sites in the receptor tetramer is believed to be critical for targeting of pathogen glycans, but the arrangement of these sites remains poorly understood. Surface force measurements between apposed lipid bilayers displaying the extracellular domain of DC-SIGN and a neoglycolipid bearing an oligosaccharide ligand provide evidence that the receptor is in an extended conformation and that glycan docking is associated with a conformational change that repositions the carbohydrate-recognition domains during ligand binding. The results further show that the lateral mobility of membrane-bound ligands enhances the engagement of multiple carbohydrate-recognition domains in the receptor oligomer with appropriately spaced ligands. These studies highlight differences between pathogen targeting by DC-SIGN and receptors in which binding sites at fixed spacing bind to simple molecular patterns.

adhesion | molecular recognition | pathogen selectivity | multivalent receptors

Pathogen recognition is the foundation of host immune response and survival against infections. In both innate and acquired immunity, pathogen recognition is achieved by host cell-surface receptors and results in a variety of downstream immune responses including opsonization and phagocytosis (1). Glycan-binding receptors in the C-type lectin superfamily form a prominent class of recognition molecules in innate immunity (2). Many C-type lectins bind arrays of glycans found on pathogens but not on host cells, thus enabling them to discriminate between self and nonself. However, some pathogens exploit this selective recognition to facilitate primary infection and subsequent proliferation in the host.

DC-SIGN (CD209), originally defined as dendritic cell-specific ICAM-3-grabbing nonintegrin, is a dendritic cell surface receptor that binds pathogen glycans. This interaction leads to internalization, followed by processing and antigen presentation (3–5). DC-SIGN binds to 2 classes of carbohydrate structures: *N*-linked high mannose oligosaccharides such as $Man_9GlcNAc_2$ and branched, fucosylated oligosaccharides (6–8). High-mannose glycans are abundant on many types of enveloped viruses including HIV, whereas fucosylated glycans are common on parasites (3). The DC-SIGN internalization pathway is exploited by HIV (HIV-1) to facilitate *trans*-infections of T cells (4, 9, 10). Other infectious agents like Ebola and Dengue viruses and *Mycobacterium tuberculosis* also use the DC-SIGN internalization pathway to infect target cells (11–13). In addition to facilitating pathogen uptake, DC-SIGN interacts with endogenous glycoproteins like intercellular adhesion molecule 2 (ICAM-2) and ICAM-3 to enable dendritic cell migration (14) and interactions between dendritic cells and T cells (5). Thus, carbohydrate recognition by DC-SIGN is important for both normal immune responses and opportunistic exploitation of the receptor by pathogens.

DC-SIGN is a tetrameric transmembrane protein, in which the extracellular domain of each subunit comprises 7-and-a-half tandem repeats of a highly conserved sequence of 23 aa, followed by a C-type carbohydrate-recognition domain (CRD) (8). Crystal structures of an isolated CRD from DC-SIGN complexed with oligosaccharide ligands reveal that the CRD forms a 1-to-1 complex with a high-mannose oligosaccharide, making multiple interactions with several of the constituent monosaccharides (6–8). This specificity places spatial constraints on the way that DC-SIGN can interact with high-mannose glycans on pathogen surfaces, because the oligosaccharide can only be accommodated in a single orientation. Similar constraints apply for binding to fucose-containing oligosaccharides (7).

The neck of DC-SIGN organizes stable tetramers and presents the CRDs in a cluster, which is believed to project from the cell surface (8). Hydrodynamic measurements and theoretical estimates place the DC-SIGN neck length between 20 and 30 nm, and a crystal structure of the CRD with a short stretch of the neck attached has been obtained (15). However, it is still not known how the structure of the neck region appropriately positions the ligand-binding sites. Because the DC-SIGN neck is considered to be important for directing the CRDs away from carbohydrate ligands in the dendritic cell membrane and toward pathogen surfaces (15), the neck configuration is likely to play a significant role in pathogen targeting.

The surface force apparatus quantifies the forces between model membranes and oriented proteins in a context that mimics interactions between cell surface receptors and glycans on target membranes. Here, force versus distance measurements are used to define the geometry of the extracellular domain of DC-SIGN, and reveal that ligand engagement is accompanied by a conformational change in the receptor. Quantified variations in the adhesion energy with ligand density further reveal the role of ligand spacing in the multivalent interactions of CRDs with ligands.

Results

Extended Conformation of DC-SIGN Measured with the Surface Force Apparatus. The surface force apparatus quantifies the force between 2 macroscopic surfaces as a function of their absolute separation, with a resolution of ±0.1 nm (16–18). In these

Author contributions: S.A.G., E.M.W., M.E.T., K.D., and D.E.L. designed research S.M., K.R., S.A.G., E.M.W., M.E.T., and K.D. performed research; S.M., K.R., M.E.T., K.D., and D.E.L. analyzed data; and S.M., M.E.T., K.D., and D.E.L. wrote the paper.

The authors declare no conflict of interest.

This article is a PNAS Direct Submission.

Freely available online through the PNAS open access option.

[1]Present address: HCI G517, Department of Materials, Eidgenössische Technische Hochschule Zürich, Wolfgang Pauli Strasse 10, 8093 Zurich, Switzerland.

[2]To whom correspondence should be addressed. E-mail: leckband@illinois.edu.

This article contains supporting information online at www.pnas.org/cgi/content/full/0901783106/DCSupplemental.

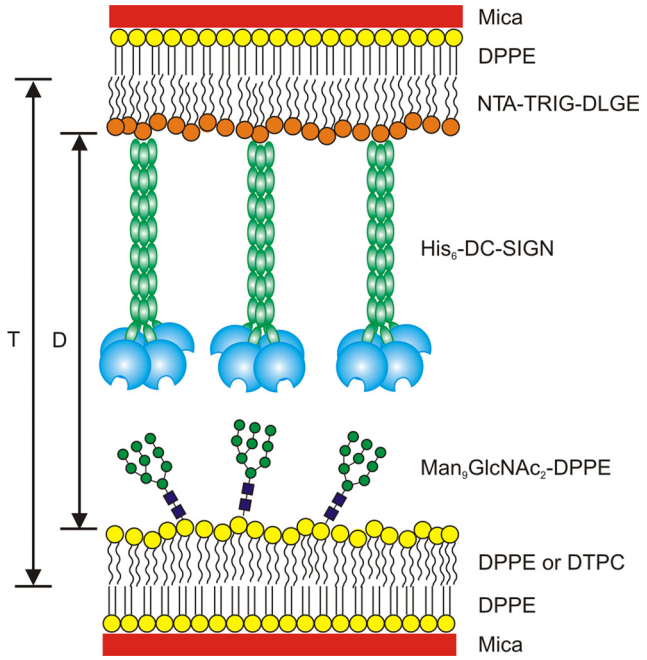

Fig. 1. Schematic of the sample configuration in the surface force apparatus experiment. Lipids used are: 1,2-dipalmitoyl-*sn*-glycero-3-phosphoethanolamine (DPPE), 1,2-ditridecanoyl-*sn*-glycero-3-phosphocholine (DTPC), and 6-[9-[2,3-bis(dodecyloxy)propyl]-3,6,9-trioxanonyl-1-oxycarboxylamino]-2-[di(carboxymethyl)-amino]-hexanoic acid (NTA-TRIG-DLGE). T is the distance between the DPPE monolayers, and D is the absolute separation between the bilayer surfaces.

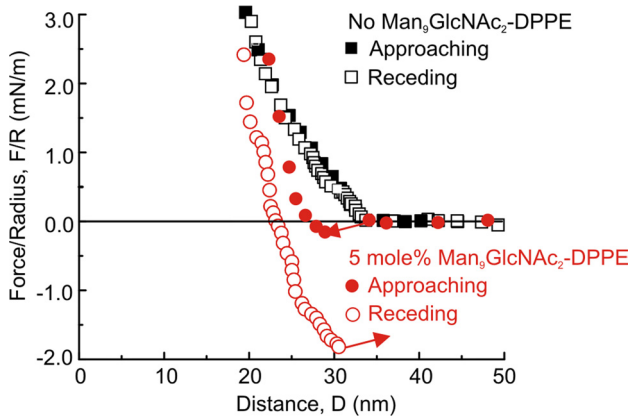

Fig. 2. Normalized force versus the distance between DC-SIGN and supported lipid bilayers in the presence and absence of neoglycolipid ligand. The black squares show the approaching (open squares) and receding (filled squares) force measurements. The red circles show the approaching (filled red) and receding (open red) force curves. The arrows show where the jump instabilities occur. At these points, the surfaces jump into or out of adhesive contact.

studies, one surface consisted of an asymmetric lipid bilayer coated with an oriented monolayer of the tetrameric extracellular domain of DC-SIGN. The protein was immobilized on nickel-chelated, nitrilo-tetra-acetate-containing lipid head groups via an N-terminal 6-histidine tag (Fig. 1). For ligand binding experiments, the outer leaflet of the opposite supported lipid bilayer contained the neoglycolipid 1,2-dipalmitoyl-*sn*-glycero-3-phosphoethanolamine (DPPE) covalently attached to an *N*-linked $Man_9GlcNAc_2$ oligosaccharide [supporting information (SI) Fig. S1].

Measurements were conducted between lipid bilayers displaying DC-SIGN and (*i*) lipid-only bilayers (control measurements) and (*ii*) bilayers containing the high-mannose oligosaccharide. Forces were measured as a function of the distance, D, between the bilayer surfaces as they were brought together and then pulled apart (Fig. 2). In the absence of the glycan, as the surfaces approach, the onset of steric repulsion occurs at $D = 32.8 \pm 0.8$ nm, and thereafter, the force increases with further decrease in distance. The onset of the repulsion corresponds to the maximum thickness of unbound DC-SIGN (D_T). Upon separation, there is no hysteresis and no adhesion, as expected in the absence of a binding interaction. See *SI Text* and Fig. S2 for additional details concerning the force measurements.

In the presence of $Man_9GlcNAc_2$-DPPE, adhesion occurs at concentrations >0.1 mol % ligand (1.5×10^3 $Man_9GlcNAc_2$-DPPE/μm^2). During approach, the surfaces jump into contact from a distance of $D_J = 35.2 \pm 1.3$ nm to a final resting position at $D = 28.1 \pm 1.2$ nm (inward-directed arrow, Fig. 2). This final resting position is significant because it is the equilibrium separation (D_{eq}) between the DC-SIGN monolayer and $Man_9GlcNAc_2$ oligosaccharide. It reflects the equilibrium steric thickness of the $Man_9GlcNAc_2$–DC-SIGN complex. There is no compressive force on the molecules, and the intersurface attraction is due solely to DC-SIGN binding to $Man_9GlcNAc_2$ head groups.

Earlier modeling of hydrodynamic measurements suggested that the neck portion of DC-SIGN forms an extended structure between 20 and 30 nm in length, although this interpretation depended on assumptions about the rigidity of the neck structure (15). The equilibrium separation D_{eq} measured with the surface force apparatus is a more direct measurement of the overall length of the extracellular portion of DC-SIGN. Allowing for a CRD diameter of 4 nm (19), the absolute length of DC-SIGN in the unbound and bound states is model-independent evidence for an extended neck length of 24 to 32 nm. Evidence from sequence analysis, circular dichroism spectroscopy, and crystallography indicate that much of the neck of DC-SIGN is in an α-helical conformation and probably forms coiled coils, although the presence of multiple proline residues suggests that there must be interruptions in such a structure (15). In a fully helical conformation, the 164-residue neck region would be expected to have a length of 25 nm. Thus, the length measurements from the surface force apparatus are consistent with a largely helical neck region without extensive folded-back segments.

Conformational Changes in DC-SIGN upon Ligand Binding. The difference between D_T and D_{eq}, which represent the protein thickness in the absence and presence of ligand, respectively, indicates that DC-SIGN undergoes a ligation-dependent conformational change. In the unbound state, DC-SIGN extends 33 nm normal to the membrane. With glycan-containing bilayers, the size of the oligosaccharide should increase the range of steric repulsion between DC-SIGN and the opposite bilayer beyond 33 nm. Instead, the 2 surfaces spontaneously jump in to adhesive contact at 28 nm (Fig. 2). This distance corresponds to a DC-SIGN-$Man_9GlcNAc_2$ complex with an end-to-end length that is 5 nm shorter than the unbound protein. The absolute decrease in the DC-SIGN thickness could exceed 5 nm, because the oligosaccharide contributes to the 28-nm length.

The jump-to-contact also suggests intrinsic flexibility in the DC-SIGN structure. Such flexibility would allow the molecules to bind at distances greater than D_{eq}. Similar behavior was measured between streptavidin monolayers and tethered biotin (20). In that case, at separations corresponding to partial extension of the polymer tethers, streptavidin and biotin bind, but the entropic chain elasticity pulls the surfaces closer together. In the

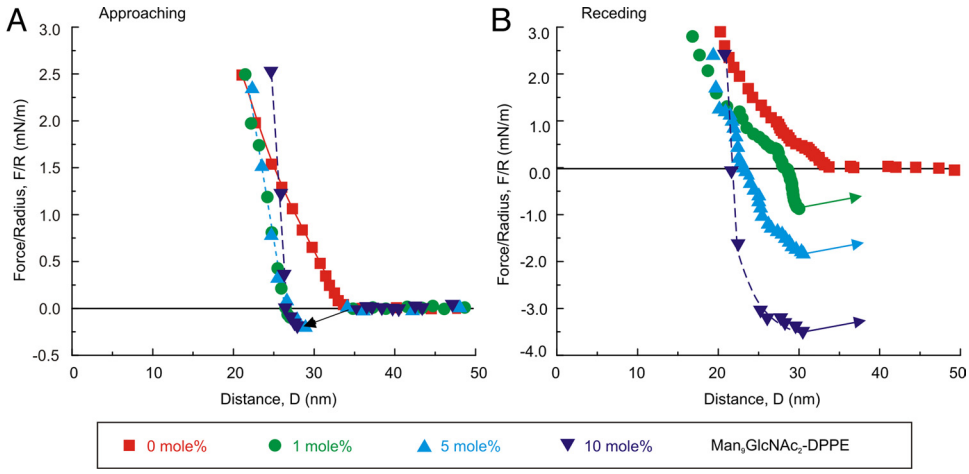

Fig. 3. Approaching (*A*) and receding (*B*) normalized force profiles between DC-SIGN and bilayers containing different densities of $Man_9GlcNAc_2$-DPPE. Data were obtained with 0 mole % (red squares), 1 mole % (green circles), 5 mole % (blue triangles), and 10 mole % (inverted blue triangles) ligand in the membrane. The lines through the data in *A* and the dashed line in *B* are shown to guide the eye.

case of DC-SIGN, a similar elasticity could arise from flexible tethers that link the CRDs to the necks.

The difference between the approach and receding curves (Fig. 2) is due to intersurface adhesion (see *SI Text*). The surfaces pull out of contact at the point of maximum adhesion at $D_{Adh} = 30.5 \pm 1.5$ nm (Fig. 2). The difference between D_{eq} and D_{Adh} is most likely due to stretching of the DC-SIGN–ligand complex under tension. This interpretation suggests that, as the surfaces are pulled apart, DC-SIGN extends by an additional 2.4 nm compared with its equilibrium, bound conformation (D_{eq}). Some contribution from reorientations of the oligosaccharide head group under tension cannot be ruled out.

The reduced compressibility of the bound DC-SIGN monolayers, relative to that of the unbound protein, provides additional evidence for the ligation-dependent structural change evident from the distance measurements. The increase in adhesion measured with fluid membranes containing increasing amounts of $Man_9GlcNAc_2$-DPPE ligand (Fig. 3) indicates an increase in the number of ligated DC-SIGN molecules, an increase in CRD occupancy per DC-SIGN tetramer, or both. However, at $D < D_{eq}$ the increase in the slopes of the advancing and receding curves observed with increasing ligand concentration further indicates an increase in the protein rigidity with increasing ligation (Fig. 3). Because the DC-SIGN density is constant, and there are no changes in the protein layer that might otherwise impact the compressibility, this trend can be attributed to the fact that an increasing number of CRDs in each tetramer become fixed in position as multiple binding sites become populated with ligands.

Two features of the force data provide direct evidence for a ligation-dependent conformational change in DC-SIGN: (*i*) the difference between D_{eq} and D_T and (*ii*) the decrease in DC-SIGN compressibility with increasing ligation. The conformational change most likely arises from changes in the link between the CRD and the end of the neck. Differences in the orientation of the CRD and neck in different crystal structures of oligomeric fragments of DC-SIGN comprising the CRD and portions of the neck suggest flexibility in this link (15). These force–distance results provide the first direct, dynamic evidence for such flexibility and its possible role in pathogen recognition. The results are consistent with the idea that the CRDs must reorient relative to the neck to accommodate binding to the outer trimannose unit of the $Man_9GlcNAc_2$ oligosaccharide, as it is presented on the membrane. This ability of the clustered CRDs in DC-SIGN to adapt to the ligand arrangement would be critical for receptors to be able to bind high-mannose oligosaccharides as they are presented on viral surfaces.

Importance of Ligand Density and Mobility for Engagement of Multiple Binding Sites. Further analysis of DC-SIGN adhesion to ligands embedded in gel- and fluid-phase membranes provides insight into interactions between multiple glycolipid ligands and the 4 CRDs in the DC-SIGN tetramer. First, at comparable ligand densities, the adhesion to ligand in fluid membranes is substantially higher than adhesion to the gel-phase membrane (Fig. 4). The much greater force required to release DC-SIGN reversibly from the fluid phase membrane suggests that more ligands are engaged. This increased occupancy of binding sites could be attributed to lateral and rotational diffusion of the ligand in the fluid membrane, which would allow ligands to diffuse into register with CRDs after initial receptor-membrane contact (see *SI Text*) (21–23). As a consequence of the ligand mobility in fluid membranes, the adhesion increased with the contact time up to a limiting plateau (Fig. S3 and Table S1).

The equilibrium adhesion energies were obtained by extrapolating the adhesion versus time curves (Fig. S3) to infinite time (*SI Text*). The values thus obtained are presented as a function

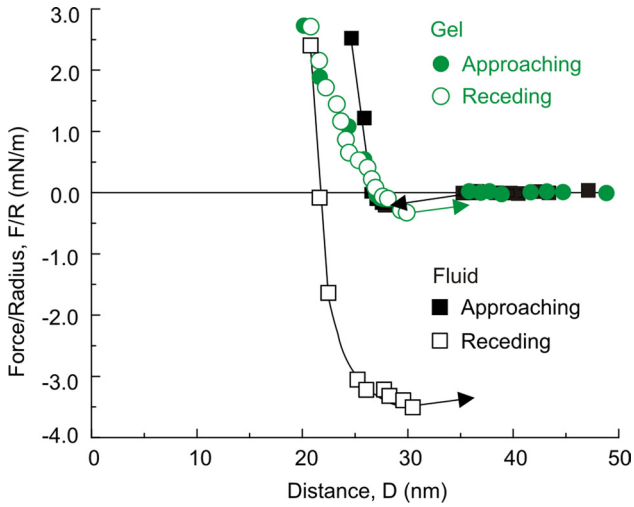

Fig. 4. Comparison of DC-SIGN binding to gel and fluid membranes containing $Man_9GlcNAc_2$-DPPE. In both cases, the ligand was present at 10 mol %.

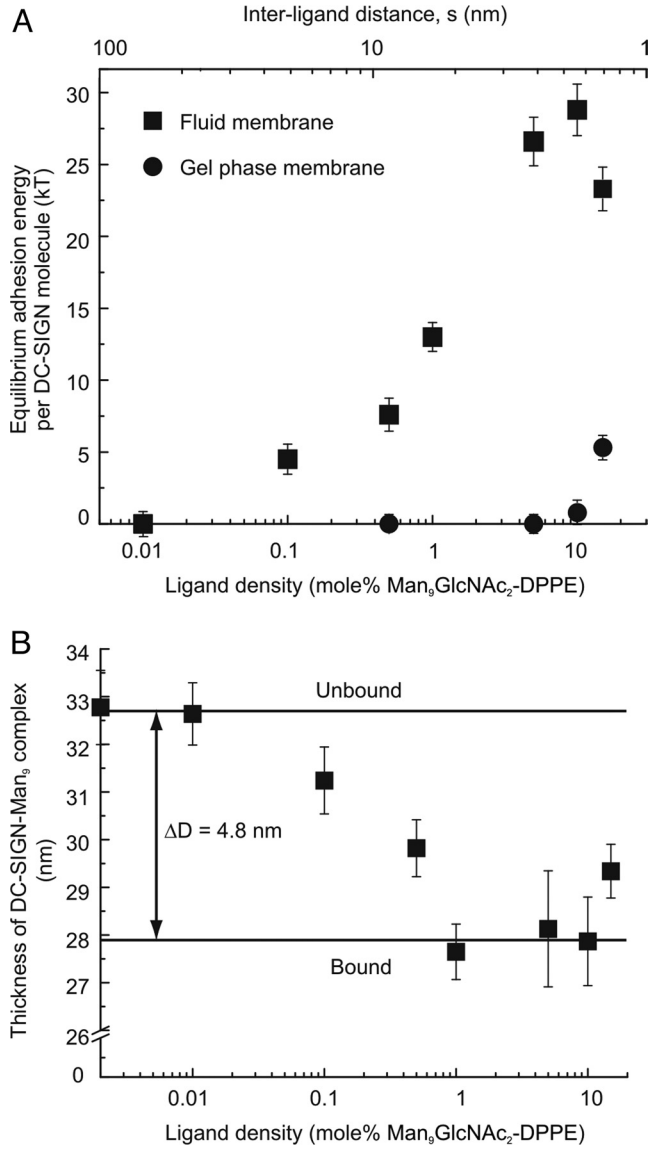

Fig. 5. Dependence of DC-SIGN–$Man_9GlcNAc_2$ complex dimensions and adhesion energy on ligand density. (*A*) DC-SIGN adhesion is presented as a function of $Man_9GlcNAc_2$-DPPE density and average interligand distance, s. (*B*) Variation in the equilibrium thickness of the bound DC-SIGN–$Man_9GlcNAc_2$ complex with $Man_9GlcNAc_2$ density. ΔD is the difference between the maximum thickness of unbound complex D_T and the equilibrium thickness of the bound complex D_{eq}. All measurements were with fluid lipid membranes.

of the ligand density (mol %) on the membrane in Fig. 5*A*. The results again highlight the difference between DC-SIGN binding to ligands in gel- and fluid-phase membranes. DC-SIGN adhesion to $Man_9GlcNAc_2$-DPPE in gel-phase membranes exhibits a sharp increase at the average interligand distance of $s = 2.4$ nm, and the adhesion energy is 0.8 ± 0.5 kT per DC-SIGN. At $s = 1.9$ nm, the average adhesion energy per protein is 5.3 ± 0.6 kT and does not change significantly with time. One interpretation of the abrupt increase in adhesion at a distinct, average spatial distribution of $Man_9GlcNAc_2$-DPPE on rigid membranes is that there is a maximum average interligand spacing that can support DC SIGN adhesion. It was not possible to position the mannose ligands at precise separation distances on the bilayers, but heteropolymer adsorption on patterned surfaces shows that pattern recognition can occur when the average spacing of adhesive monomers matches the average distribution of surface binding sites (24). In this case, the interligand distance likely underestimates the true inter-CRD spacing because the binding site of each CRD in DC-SIGN interacts selectively with the branch residue in the outer trimannose unit of the $Man_9GlcNAc_2$ oligosaccharide (6, 7). Binding will only occur with certain orientations of the ligand. In the gel phase, the constrained rotational motion of the glycan would limit the number of ligands able to bind CRDs. Nevertheless, the abrupt onset of adhesion to immobile ligands at a defined ligand density rather than a gradual increase in adhesion, which would be expected as CRDs become successively populated, suggests that the spatial distribution of ligands constrains DC-SIGN recognition.

In contrast to the interaction with gel-phase membranes, DC-SIGN adhesion to ligands on fluid membranes, where the mobile ligands can adapt to the CRD distribution on the time scale of the measurement, not only increases with intersurface contact time, but gradually reaches a higher limiting adhesion plateau with increasing ligand density (Fig. S3*A*). The maximum adhesion energy is at 10 mol % $Man_9GlcNAc_2$-DPPE. The estimated equilibrium adhesion energy per DC-SIGN molecule is 28.8 ± 1.4 kT, which is 36 times greater than on a gel membrane at the same average ligand density. The large, lipid-bound DC-SIGN is less mobile than the glycolipids, so the time-dependent increase in adhesion (Fig. S3*B*) is attributed mainly to the lateral diffusion of the $Man_9GlcNAc_2$-DPPE.

The mobility of individual ligands relaxes spatial constraints for multivalent receptor binding (22, 23). The apparent optimum interligand spacing (ligand density) on fluid membranes (Fig. 5*A*) is influenced both by the spatial constraints of the receptor and by the receptor-surface contact time. The adhesion drop at ligand densities >10 mol % $Man_9GlcNAc_2$-DPPE is probably due to ligand crowding, which would sterically impede ligand interactions with the CRDs (25–28).

The variation in the equilibrium thickness of the DC-SIGN–glycan complex as a function of the ligand density provides further insight into the conformational change in DC-SIGN due to ligand binding. At low ligand density, the adhesion is low, and the steric thickness of the DC-SIGN monolayer is $D_T = 32.8 \pm 0.8$ nm (Fig. 5*B*). This is the same value as the thickness of the unbound DC-SIGN. The average thickness of the DC-SIGN monolayer then decreases gradually from 30 to 28 nm with increasing ligand density and corresponding adhesion. The measured complex length then remains relatively constant at a limiting value of 27.9 ± 0.2 nm until the ligand crowding effect again reduces the adhesion. The range of the repulsion reflects the entire DC-SIGN population in the contact region, so it is not possible to distinguish between a gradual conformational change with increasing CRD occupancy versus an average between 2 conformational states in which their relative populations change with changing ligation. Nevertheless, there is a clear change in the DC-SIGN conformation that coincides with increasing ligand binding to the CRDs.

Discussion

The results of surface force measurements on DC-SIGN identify one way that this receptor may interact with glycans on pathogens such as enveloped viruses. A picture of DC-SIGN interactions with pathogen membranes that differs significantly from the proposed model for recognition by other glycan-binding receptors emerges from the demonstration (*i*) that a conformational change in the receptor accompanies ligand engagement and (*ii*) that a significant degree of mobility in the arrangement of glycan ligands is required to achieve optimal binding. These features highlight contrasts between potential mechanisms of DC-SIGN binding to viruses and the mode of action of mannose-binding protein, a commonly used paradigm for innate immune recognition of bacterial and fungal surfaces.

The ligand-binding site in a CRD in mannose-binding protein broadly accommodates terminal mannose, *N*-acetylglucosamine and fucose residues. Binding to individual monosaccharides is very weak and is not enhanced by interactions with subterminal residues in a glycan (29). High-avidity interactions therefore require engagement of monosaccharide-binding sites in multiple CRDs. Clusters of 3 of these CRDs are held in a rigid orientation facing in 1 direction, so they are able to bind to sugars displayed on surfaces. Because of the fixed spacing of ≈5 nm between the sugar-binding sites, a high density of potential monosaccharide partners is required on a target surface to ensure that some will be spaced appropriately for interaction with the CRDs (30). Pathogen selectivity is therefore linked directly to the spatial organization of the CRDs, and derives from putative pattern matching between the arrangement of CRDs on mannose-binding protein and the carbohydrate ligand array (30).

The much more extensive ligand-binding site in DC-SIGN results in higher-affinity 1-to-1 interactions with specific glycans, although engagement of such ligands is more geometrically constrained (7). The flexibility in DC-SIGN revealed by these force–distance measurements relaxes the strict requirement for pattern matching seen in the mannose-binding protein. This flexibility allows multiple CRDs in a tetramer to interact with more complex but more sparsely spaced glycan ligands on a membrane, to effect strong adhesion. The total adhesion between DC-SIGN and the glycolipid-coated surface reflects the capacity of DC-SIGN to adapt to the arrangement of the target ligands on the membrane such that all of the CRDs can interact with ligands. The studies with fluid- and gel-phase membranes indicate that even with this degree of flexibility in DC-SIGN, some mutability of ligand spacing is still required to achieve optimal multivalent adhesion.

Mobility of the neoglycolipid targets in the fluid-phase membranes may mimic flexibility in glycans attached to viral glycoproteins. Nevertheless, the ability of the CRDs in DC-SIGN to reorient would still be critical for interactions with glycans on viral surfaces, because these would be presented in multiple orientations on glycoproteins rather than on a planar lipid array. When the glycans are tethered to glycoproteins such as gp120 on HIV, similar structural changes in the link between the CRD and the neck of DC-SIGN are expected to further enhance the affinity.

Even with an extended binding site interacting with an oligosaccharide ligand, the dissociation constant between DC-SIGN and an individual high-mannose oligosaccharide in solution is only ≈0.2 mM (8). It is well established that multivalent interactions of a receptor oligomer with multiple ligands on a surface result in dramatically enhanced affinity (31), although the essentially irreversible nature of such interactions has made it difficult to determine actual affinities in a membrane context. Thus, an important insight resulting from these surface-force apparatus measurements is the quantification of the enhanced binding energy achieved through multivalency. Despite the weak individual protein–glycan interactions, the maximum estimated adhesion energy per DC-SIGN tetramer measured in the surface force apparatus is 28 kT. For comparison, an adhesion energy of 8 kT was measured between the T cell adhesion receptor CD2 and CD58, which have a dissociation constant of 9 μM (32). The adhesion energies are relevant to binding between cell surfaces and pathogens, but they cannot be directly related to solution binding affinities, in part because of the restricted mobility and loss of entropy relative to the soluble species. The adhesion of DC-SIGN nevertheless exceeds what might be expected from comparisons with similarly measured adhesion energies of other receptors with much higher binding affinities than that of a single CRD for glycan.

The differences in the molecular properties of mannose-binding protein and DC-SIGN explain differences in their selectivity for pathogens. Mannose-binding protein binds to bacterial and fungal surfaces that consist of dense and repetitive arrays of terminal monosaccharide ligands, whereas DC-SIGN binds particularly well to closely spaced oligosaccharides on the envelopes of viruses and membranes of parasites (2, 33). The fact that simple pattern matching is not a universal principle in host–pathogen interactions is particularly important in the context of drugs designed to block viral infection. In the mannose-binding protein type of situation, the pattern-matching hypothesis suggests that competing ligands assembled on appropriate structural templates could block interactions with targets in a therapeutically useful way, because high-affinity binding and strong adhesion occur only when the ligand template matches the spatial arrangement of receptor sites (33–35). In other cases, polyvalent inhibitors were developed, based on a model in which recognition occurs when the average spacing between the binding centers matches the average interligand distance (24). Such polyvalent inhibitors of anthrax toxin (36), Shiga and Shiga-like toxins (37, 38), enterotoxin (39), and cholera toxin (23, 40) exhibit affinities enhanced 10^2- to 10^6-fold when pattern-matched to their targets. Yet even greater enhancements in affinity for Shiga were achieved by designing multivalent ligands with spacings that exactly matched the distances between binding sites (37). The results reported here suggest that a similar approach to designing inhibitors of DC-SIGN would have to take into account the flexibility of the receptor and the need for flexibility in the spacing and orientation of glycans in a competing ligand.

Methods

Lipids. 1,2-dipalmitoyl-*sn*-glycero-3-phosphoethanolamine (DPPE) and 1,2-ditridecanoyl-*sn*-glycero-3-phosphocholine (DTPC) were purchased from Avanti Polar Lipids. 6-[9-[2,3-bis(dodecyloxy)propyl]-3,6,9-trioxanonyl-1-oxycarboxylamino]-2-[di(carboxymethyl)-amino]-hexanoic acid (NTA-TRIG-DLGE) (Fig. S1) was custom synthesized by Northern Lipids.

DC-SIGN Immobilization on Supported Planar Lipid Bilayers. The soluble extracellular domain of DC-SIGN, engineered with an N-terminal hexahistidine tag (*SI Text*), was immobilized on planar, asymmetric lipid bilayers supported on freshly cleaved mica sheets (Fig. 1). First a DPPE monolayer was deposited on the mica surface at 43 Å^2 per lipid (41) by Langmuir–Blodgett deposition. A second lipid layer containing 100% NTA-TRIG-DLGE was deposited onto the first layer at a constant surface pressure of 35 mN/m (≈65 Å^2 per lipid). The subphase containing 20 mM Hepes, 50 mM $NaNO_3$, 3 mM $Ca(NO_3)_2$, and 50 μM $NiSO_4$ at pH 7.8 (Buffer A) was maintained at 21 °C. Full details are provided in *SI Text*. The resultant supported bilayer was kept under the Buffer A at all times. The bilayer was then incubated for 1.5 h with 0.5 μM His_6-DC-SIGN in Buffer A. The determination of the surface density of DC-SIGN tetramers immobilized on the bilayers is described in *SI Text*.

$Man_9GlcNAc_2$-DPPE Model Membrane Preparation. Asymmetric bilayers containing $Man_9GlcNAc_2$-DPPE oligosaccharide supported on atomically flat mica sheets were prepared by Langmuir–Blodgett deposition (41). The synthesis of the $Man_9GlcNAc_2$-DPPE neoglycolipid and preparation of the supported lipid bilayers are described in *SI Text*. The first layer is a DPPE monolayer (43 Å^2 per lipid) above (Fig. 1). The outer monolayer containing mixtures of $Man_9GlcNAc_2$-DPPE and either DPPE (gel, $T_m > 21$ °C) or DTPC (fluid, $T_m < 21$ °C) was deposited at a constant surface pressure of 35 mN/m, which corresponds to 44.1 ± 0.9 Å^2/DPPE and 65.4 ± 0.8 Å^2/DTPC. The molar concentrations of DPPE, DTPC, and Man_9-$GlcNAc_2$-DPPE in the stock solutions were determined with the Bartlett phosphorus assay (42). The average area per lipid in the outer monolayer and the mole fraction of ligand-modified lipids together determine the sugar distribution on the bilayer surface. For example, in the gel phase, ethanolamine head groups occupy 44.1 Å^2 so that the average distance between the lipid centers would be $s = 2\sqrt{\text{Area}/\pi} = 2\sqrt{44.1/\pi} = 7.4$ Å. However, when the gel phase lipid monolayer contains 10 mol % $Man_9GlcNAc_2$-DPPE, then the average distance between the $Man_9GlcNAc_2$ oligosaccharides would be $s = 2\sqrt{441\ \text{Å}^2/\pi} = 23.7$ Å.

The bilayers containing DC-SIGN and $Man_9GlcNAc_2$-DPPE were placed in a Mark III surface-force apparatus chamber, which contained buffer (16) (Fig. 1). All measurements were performed at 21 ± 0.2 °C.

Surface-Force Measurements. The sample configuration for the surface-force experiments is given in Fig. 1. The surface-force apparatus quantifies the force between the lipid bilayers displaying DC-SIGN and $Man_9GlcNac_2$ as a function of the absolute separation distance (D) between them. The absolute separation between the supported bilayers is defined as $D = T - (T_{NTA\text{-}TRIG\text{-}DLGE} + T_{DPPE/DTPC})$ where T is the calibrated distance between the DPPE monolayers, and $T_{NTA\text{-}TRIG\text{-}DLGE}$ is the thickness of the NTA-TRIG-DLGE monolayer (Fig. 1) (43). $T_{DPPE/DTPC}$ is the thickness of the matrix lipid (DPPE or DTPC) (41) and does not include the thickness of $Man_9GlcNAc_2$ head group. Therefore, $D = 0$ corresponds to the contact between the NTA-TRIG-DLGE membrane and the ligand-free lipid membrane.

The force between the surfaces is determined from the deflection of a sensitive leaf spring supporting one of the samples. The force, normalized by the geometric average radius of the hemicylindrical disks supporting the samples ($R = \sqrt{R_1R_2}$), is determined within $\Delta F/R = \pm 0.1$ mN/m $= 0.1$ mJ/m^2 (44). Thus, the normalized force between curved macroscopic substrates (F_c) is related to the energy per unit area between 2 equivalent flat plates (E_f) by the Derjaguin approximation: $F_c/R = 2\pi E_f$ (44).

The adhesion energy per unit area (E_a) is determined from the force to separate the adhesive layers (F_a): the maximum attractive force. The Derjaguin–Müller–Toporov theory (44) relates F_a to the adhesion energy per unit area by $E_a = F_a/2\pi R$. Further normalizing E_a by the DC-SIGN surface coverage accounts for differences in protein densities across experiments. More details regarding the force measurements are given in *SI Text*.

ACKNOWLEDGMENTS. We thank Dawn Torgersen and Brian Matthews for preparation of the $Man_9GlcNAc_2$ oligosaccharide. This work was supported by the Reid T. Milner Professorship (D.E.L.) and by Wellcome Trust Grant 075565 (to K.D. and M.E.T.).

1. Janeway C, Jr, Medzhitov R (2002) Innate immune recognition. *Annu Rev Immunol* 20:197–216.
2. Cambi A, Figdor C (2005) Levels of complexity in pathogen recognition by C-type lectins. *Curr Opin Immunol* 17:345–351.
3. Appelmelk B, et al. (2003) Cutting edge: Carbohydrate profiling identifies new pathogens that interact with dendritic cell-specific ICAM-3-grabbing nonintegrin on dendritic cells. *J Immunol* 170:1635–1639.
4. Geijtenbeek T, et al. (2000) DC-SIGN, a dendritic cell-specific HIV-1-binding protein that enhances trans-infection of T cells. *Cell* 100:587–597.
5. Geijtenbeek T, et al. (2000) Identification of DC-SIGN, a novel dendritic cell-specific ICAM-3 receptor that supports primary immune responses. *Cell* 100:575–585.
6. Feinberg H, Mitchell D, Drickamer K, Weis W (2001) Structural basis for selective recognition of oligosaccharides by DC-SIGN and DC-SIGNR. *Science* 294:2163–2166.
7. Guo Y, et al. (2004) Structural basis for distinct ligand-binding and targeting properties of the receptors DC-SIGN and DC-SIGNR *Nat Struct Mol Biol* 11:591–598.
8. Mitchell DA, Fadden AJ, Drickamer K (2001) A novel mechanism of carbohydrate recognition by the C-type lectins DC-SIGN and DC-SIGNR. Subunit organization and binding to multivalent ligands. *J Biol Chem* 276:28939–28945.
9. Pohlmann S, Baribaud F, Doms R (2001) DC-SIGN and DC-SIGNR: Helping hands for HIV. *Trends Immunol* 22:643–646.
10. van Kooyk Y, Geijtenbeek T (2003) DC-SIGN: Escape mechanism for pathogens. *Nat Rev Immunol* 3:697–709.
11. Simmons G, et al. (2003) DC-SIGN and DC-SIGNR bind Ebola glycoproteins and enhance infection of macrophages and endothelial cells. *Virology* 305:115–123.
12. Tassaneetrithep B, et al. (2003) DC-SIGN (CD209) mediates Dengue virus infection of human dendritic cells. *J Exp Med* 197:823–829.
13. Tailleux L, et al. (2003) DC-SIGN is the major *Mycobacterium tuberculosis* receptor on human dendritic cells. *J Exp Med* 197:121–127.
14. Geijtenbeek T, et al. (2000) DC-SIGN-ICAM-2 interaction mediates dendritic cell trafficking. *Nat Immunol* 1:353–357.
15. Feinberg H, et al. (2005) Extended neck regions stabilize tetramers of the receptors DC-SIGN and DC-SIGNR. *J Biol Chem* 280:1327–1335.
16. Israelachvili J, Adams G (1978) Measurement of forces between two mica surfaces in aqueous electrolyte solutions in the range 0–100 nm. *J Chem Soc Faraday Trans I* 75:975–1001.
17. Israelachvili J (1992) Adhesion forces between surfaces in liquids and condensable vapours. *Surf Sci Rep* 14:110–159.
18. Israelachvili J (1973) Thin film studies using multiple-beam interferometry. *J Colloid Interface Sci* 44:259–272.
19. Weis WI, et al. (1991) Structure of the calcium-dependent lectin domain from a rat mannose-binding protein determined by MAD phasing. *Science* 254:1608–1615.
20. Wong J, et al. (1997) Direct measurement of a tethered ligand-receptor interaction potential. *Science* 275:820–822.
21. Chan P, et al. Influence of receptor lateral mobility on adhesion strengthening between membranes containing LFA-3 and CD2. *J Cell Biol* 115:245–255, 1991.
22. Leckband D, Schmitt F, Israelachvili J, Knoll W (1994) Direct force measurements of specific and nonspecific protein interactions. *Biochemistry* 33:4611–4624.
23. Rai P, et al. (2006) Statistical pattern matching facilitates the design of polyvalent inhibitors of anthrax and cholera toxins. *Nat Biotechnol* 24:582–586.
24. Golumbfskie A, Pande V, Chakraborty A (1999) Simulation of biomimetic recognition between polymers and surfaces. *Proc Natl Acad Sci USA* 96:11707–11712.
25. Aisenbrey C, Bechinger B, Grobner G (2008) Macromolecular crowding at membrane interfaces: Adsorption and alignment of membrane peptides. *J Mol Biol* 375:376–385.
26. Johnson C, et al. (2003) Engineered protein A for the orientational control of immobilized proteins. *Bioconjug Chem* 14:974–978.
27. Soong R, Macdonald P (2007) PEG molecular weight and lateral diffusion of PEG-ylated lipids in magnetically aligned bicelles. *Biochim Biophys Acta* 1768:1805–1814.
28. Stankowski S (1983) Large-ligand adsorption to membranes II. Disc-like ligands and shape dependence at low saturation. *Biochim Biophys Acta* 735:352–360.
29. Lee RT, et al. (1991) Ligand-binding characteristics of rat serum-type mannose-binding protein (MBP-A): Homology of binding site architecture with mammalian and chicken hepatic lectins. *J Biol Chem* 266:4810–4815.
30. Weis W, Drickamer K (1994) Trimeric structure of a C-type mannose-binding protein. *Structure (London)* 2:1227–1240.
31. Dam TK, Brewer C (2008) Effects of clustered epitopes in multivalent ligand-receptor interactions. *Biochemistry* 47:8470–8476.
32. Bayas M, et al. (2007) Impact of salt bridges on the equilibrium binding and adhesion of human CD2 and CD58. *J Biol Chem* 282:5589–5596.
33. Holmskov U, Thiel S, Jensenius J (2003) Collections and ficolins: Humoral lectins of the innate immune defense. *Annu Rev Immunol* 21:547–578.
34. Kiessling L, Gestwicki J, Strong L (2006) Synthetic multivalent ligands as probes of signal transduction. *Angew Chem Int Ed Engl* 45:2348–2368.
35. Weis W, Drickamer K (1996) Structural basis of lectin-carbohydrate recognition. *Annu Rev Biochem* 65:441–473.
36. Mourez M, et al. (2001) Designing a polyvalent inhibitor of anthrax toxin. *Nat Biotechnol* 19:958–961.
37. Kitov PI, et al. (2000) Shiga-like toxins are neutralized by tailored multivalent carbohydrate ligands. *Nature* 403:669–672.
38. Kitov PI, Bundle DR (2003) On the nature of the multivalency effect: A thermodynamic model. *J Am Chem Soc* 125:16271–16284.
39. Fan E, et al. (2000) High-affinity pentavalent ligands of *Escherichia coli* heat-labile enterotoxin by modular structure-based design. *J Am Chem Soc* 122:2663–2664.
40. Zhang Z, et al. (2002) Solution and crystallographic studies of branched multivalent ligands that inhibit the receptor-binding of cholera toxin. *J Am Chem Soc* 124:12991–12998.
41. Marra J, Israelachvili J (1985) Direct measurements of forces between phosphatidylcholine and phosphatidylethanolamine bilayers in aqueous electrolyte solutions. *Biochemistry* 24:4608–4618.
42. Bartlett G (1959) Phosphorus assay in column chromatography. *J Biol Chem* 234:466–468.
43. Martel L, et al. (2002) X-ray reflectivity investigations of two-dimensional assemblies of C-cadherins: First steps in structural and functional studies. *J Phys IV France* 12:365–377.
44. Israelachvili J (1992) *Intermolecular and Surface Forces* (Academic, New York).